superlattice reflections due to the incident-beam rocking are useful for determining the phases of the structure factors of the surface layer.

We proposed in a previous paper to image surface structures at atomic resolution based on a computer simulation (Takayanagi & Honjo, 1980). As seen from (5) and (6), we can obtain structure images at a special thickness of the bulk crystal, $z = 1/Y$, since the phases of the superlattice reflections depend on F_s'. It is very useful for phase determination to detect displacement of lattice fringes in high-resolution images obtained at crystal thicknesses of 1/4 and 1/2 of the extinction distance, from which we know the relative phase of F_s and F_s'.

We propose, thus, combined use of diffraction and/or high-resolution microscopy for phase determination of structure factors, in addition to kinematical intensity analyses such as those previously done for the Si(111) 7×7 reconstructed surface (Takayanagi, Tanishiro, M. Takahashi & S. Takahashi, 1985; Takayanagi, Tanishiro, S. Takahashi & M. Takahashi, 1985).

The present author expresses his sincere thanks to Dr K. Kambe for critical reading of the manuscript and discussions.

References

CHANG, S. L. (1984). *Multiple Diffraction of X-rays in Crystals*, p. 114. Berlin: Springer-Verlag.
COWLEY, J. M. (1975). *Diffraction Physics*, p. 225. Amsterdam: North-Holland.
HOWIE, A. (1970). *Modern Diffraction and Imaging Techniques in Material Science*, edited by S. AMELINCKX, R. GEBERS, G. REMAUT & J. VAN LANDUYT, p. 295. Amsterdam: North-Holland.
KAMBE, K. (1957). *J. Phys. Soc. Jpn*, **12**, 13-31.
RADI, G. (1970). *Acta Cryst.* A**26**, 41-56.
TAKAYANAGI, K. & HONJO, G. (1980). Proc. of 8th Int. Vacuum Congress, Vol. 1, p. 267. Paris: Société Française du Vide.
TAKAYANAGI, K., TANISHIRO, Y., TAKAHASHI, M. & TAKAHASHI, S. (1985). *J. Vac. Sci. Technol.* A**3**, 1502-1506.
TAKAYANAGI, K., TANISHIRO, Y., TAKAHASHI, S. & TAKAHASHI, M. (1985). *Surf. Sci.* **164**, 367-392.
TANISHIRO, Y. & TAKAYANAGI, K. (1989). *Ultramicroscopy*, **27**, 1-8.

Acta Cryst. (1990). A**46**, 86-94

Monte Carlo Calculation of A_3B (111) Ordering Transition and Surface X-ray Intensities

BY X.-M. ZHU AND H. ZABEL*

Department of Physics and Materials Research Laboratory, University of Illinois at Urbana-Champaign, 1110 W. Green Street, Urbana, IL 61801, *USA*

(*Received* 29 *March* 1989; *accepted* 30 *August* 1989)

Abstract

A Monte Carlo simulation of an ordering phase transition in the surface region of a f.c.c.-type A_3B binary alloy is reported. The main emphasis of this simulation is the evaluation of short and long-range-order correlations near the surface which are used for calculating X-ray intensities under grazing-incident-angle conditions. These calculations suggest effective ways of conducting surface diffraction experiments on order–disorder phase transitions. The simulation results are also compared with available experimental data.

I. Introduction

The effect of the surface when a system undergoes a bulk first-order phase transition has been studied recently in much detail by various theoretical methods, including mean-field approximation (Lipowsky & Speth, 1983; Lipowsky, 1984), Landau free-energy expansion (Mejia-Lira, Benneman & Moran-Lopez, 1985), and cluster variation for semi-infinite systems (Sanchez & Moran-Lopez, 1985). The thick-film case was examined by use of a continuous Landau free-energy expansion (Lipowsky & Gompper, 1984; Sornette, 1985), and the thin-film case in the Bragg–Williams approximation (Sanchez, Mejia-Lira & Moran-Lopez, 1986). These calculations were carried out for both magnetic and binary alloy systems and focused on the order-parameter profiles in the vicinity of the phase transition. This previous work encouraged us to investigate surface effects on the order–disorder transition of A_3B-type alloys by using Monte Carlo (MC) simulation methods. MC simulations of the bulk phase transition have been carried out in the past by Golosov & Dudka (1973) and by Polgreen (1985). More recently MC simulations of three-dimensional systems including surface effects (Gompper & Kroll, 1988) have emerged.

* Present address: Fakultät für Physik und Astronomie, Experimentalphysik IV, Ruhr Universität Bochum, Universitätsstrasse 150, D-4630 Bochum 1, Federal Republic of Germany.

0108-7673/90/020086-09$03.00

In recent years experiments have been reported on the surface ordering transition of binary alloys *via* low-energy electron scattering (LEED) (McRae & Malic, 1984) and spin-polarized electron scattering (SPLEED) (Jamison, Lind, Dunning & Watters, 1985; Alvarado, Campagna, Fattah & Uelhoff, 1987). In those experiments, the order parameter of the first layer was measured and compared with theoretical predictions. However, electron scattering experiments are limited to information on the topmost layer. Strong interactions between electron beams and the material probed give rise to multiple scattering events which are difficult to analyze. The newly developed grazing-incidence X-ray scattering technique (Eisenberg & Marra, 1981; Als-Nielsen, 1986) has important advantages over electron scattering since it yields information on ordering effects in surface and subsurface layers and is capable of providing information on both long-range- and short-range-order correlations which cannot be distinguished by electron scattering. Two independent grazing-incidence X-ray scattering experiments have been carried out so far on the order–disorder transition of the Cu_3Au (111) surface (Zhu, Feidenhans'l, Zabel, Als-Nielsen, Du, Flynn & Grey, 1988) and (100) surface (Dosch, Mailander, Lied, Peisl, Grey, Johnson & Krummacher, 1988). From our MC results on the correlation function we have calculated X-ray intensities which will be compared with experimentally obtained intensities.

Previous calculations showed that the phase transition differs depending on the surface orientation. In this paper we only consider the (111) surface of Cu_3Au-type binary alloys. We will discuss the results of our MC simulation in terms of order-parameter profiles similar to the recent work by Gompper & Kroll (1988). In addition, we provide concentration and short-range-order-parameter profiles for temperatures both above and below the ordering temperature. We have also simulated the X-ray intensities expected for scattering under grazing-incident-angle conditions.

II. Theroretical procedure

1. *The model and the Monte Carlo procedure*

Cu_3Au-type binary alloys in the ordered phase exhibit a face-centered-cubic structure with Cu atoms occupying face-centered sites (β sites) and Au atoms sitting on the corners (α sites). If we consider only the nearest-neighbor interaction, we can write the Hamiltonian (de Fontaine, 1979)

$$H = -J \sum_{ij} S_i S_j - H \sum_i S_i. \qquad (1)$$

Here S_i are the pseudospin variables with values $+1(-1)$ if site i is occupied by atom A (or B). $J = \frac{1}{4}(V_{AA} + V_{BB} - 2V_{AB})$, where V_{AA}, V_{BB}, V_{AB} are the pairwise interaction potentials. The effective field is given by $H = \frac{1}{2}(\mu_A - \mu_B)$, where μ_A, μ_B are the chemical potentials for each kind of atom. We note that the Hamiltonian in (1) is the Hamiltonian of a rigid lattice and does not take size effects into account. In the actual Cu_3Au system it is well known that size effects can be important for interpreting short-range-order parameters, which will be discussed further below (Schwartz & Cohen 1965; Chen, Comstock & Cohen, 1979).

In the presence of a surface, we assume that the interaction between atoms differs from their bulk value J only in the case that both atoms are located in the surface layer. We denote the interaction between two nearest surface atoms as J_1. Then, the Hamiltonian of a binary alloy system including a surface layer can be written as

$$H = -J \sum_{ij} S_i S_j - J_1 \sum_{i^* j^*} S_{i^*} S_{j^*} - H \sum_i S_i - H_1 \sum_{i^*} S_{i^*}, \qquad (2)$$

where $H_1 = \frac{1}{2}(E_A - E_B)$, and E_A, E_B are the segregation energies for each kind of atom. The sums i^*, j^* go only over the atoms in the surface layer.

The MC simulation was carried out using $24 \times 24 \times 30$ lattice sites having a [111] orientation in the z direction. The calculation was performed in two steps. First, we used the Hamiltonian for the bulk (1) and applied periodic boundary conditions in all three directions to simulate the phase transition in the bulk. This was done for the following reasons: first, to compare our MC results with well established experimental data which provide a quality control of our simulation; and, secondly, to enable us later to discriminate between surface and bulk effects. Subsequently, using the Hamiltonian of (2) we applied periodic boundary conditions in the xy plane only, while leaving two free surfaces in the z direction. In both cases we started with initial conditions characterized by a completely ordered structure and used spin-exchange dynamics to bring the system to equilibrium (Binder, 1986). In the spin-exchange simulation the second term (1) is a constant and can be ignored. The system reached equilibrium after 30 to 80 Monte Carlo steps depending on the temperature. All physical quantities were averaged over many Monte Carlo steps after the system reached equilibrium to ensure proper statistical averages.

2. *Order parameters*

The order parameter of the order–disorder phase transition in question is defined as

$$\eta = p_A^\alpha - p_A^\beta = p_B^\alpha - p_B^\beta, \qquad (3)$$

where $p_I^\alpha (p_I^\beta)$ are the probabilities of finding an atom $I(A$ or $B)$ on an α (or β) site.

The order parameter is calculated in the following way:

$$\eta = (\langle S\rangle_\alpha - m)/(1-m), \tag{4}$$

where $m = \sum_i S_i/N = \frac{1}{2}$ is the total spin divided by the number of lattice sites. $\langle S\rangle_\alpha$ is the average spin of the α site averaged over Monte Carlo steps after attaining equilibrium.

In the presece of a surface, the order parameter becomes z dependent:

$$\eta(z) = p_A^\alpha(z) - p_A^\beta(z) = p_B^\alpha(z) - p_B^\beta(z), \tag{5}$$

and is defined for each layer by

$$\eta(z) = [\langle S\rangle_\alpha(z) - m(z)]/[1-m(z)]. \tag{6}$$

3. *Bulk X-ray intensities*

In order to calculate X-ray intensities, additional information other than the order parameter is required. The differential scattering cross section for an X-ray scattered off a bulk crystal is (Warren, 1969)

$$\begin{aligned} d\sigma/d\Omega &= A_0 \sum_{ij} \langle f_i f_j\rangle \exp(i\mathbf{Q}\mathbf{R}_{ij}) \\ &= A_0 \sum_{ij} \langle f_i\rangle\langle f_j\rangle \exp(i\mathbf{Q}\mathbf{R}_{ij}) \\ &\quad + A_0 \sum_{ij} (\langle f_i f_j\rangle - \langle f_i\rangle\langle f_j\rangle)\exp(i\mathbf{Q}\mathbf{R}_{ij}) \\ &= A_0 S(\mathbf{Q}), \end{aligned} \tag{7}$$

where $\mathbf{Q}$ is the scattering vector with magnitude $|\mathbf{Q}| = (4\pi/\lambda)\sin\theta$, and $\mathbf{R}_{ij}$ are postion vectors for the distance between the atoms i and j. A_0 collects all extrinsic factors including the classical electron radius and geometry factors. Later we evaluate only $S(\mathbf{Q})$. The form factor f_i is equal to f_A (or f_B) if site i is occupied by atom A (or B), and f_A, f_B are the atomic form factors of the atoms A and B. f_i can be expressed in terms of the pseudospin S_i as

$$\begin{aligned} f_i &= \tfrac{1}{2}(1+S_i)f_A + \tfrac{1}{2}(1-S_i)f_B \\ &= \bar{f} + \tfrac{1}{2}\tilde{f}(S_i - m), \end{aligned} \tag{8}$$

where $\bar{f} = c_A f_A + c_B f_B$ is the averaged structure factor, c_A and c_B are the atomic concentrations, and $\tilde{f} = f_A - f_B$. Rewriting $S(\mathbf{Q})$ with the definition of (8), we obtain

$$S(\mathbf{Q}) = |\sum_i \bar{f}\exp(i\mathbf{Q}\mathbf{R}_i) + \tfrac{1}{2}\sum_i \tilde{f}(S_i - m)\exp(i\mathbf{Q}\mathbf{R}_i)|^2. \tag{9}$$

The first term represents the intensity of the fundamental reflections and the second term the superlattice reflections. In this discussion we have neglected thermal and static Debye-Waller factors as well as phonon diffuse scattering.

Using a superlattice wave vector $\boldsymbol{\tau}$, with the property $\exp(i\boldsymbol{\tau}\mathbf{R}) = +1(-1)$ when $\mathbf{R}$ is at an $\alpha(\beta)$ site, $S'(\mathbf{Q})$ due to the ordering of A and B atoms can be written as

$$\begin{aligned} S'(\mathbf{Q}) &= \tfrac{1}{4}\tilde{f}^2 |\sum_i \eta \exp[i(\mathbf{Q}+\boldsymbol{\tau})\mathbf{R}_i]|^2 \\ &\quad + \tfrac{1}{4}\tilde{f}^2 \sum_{ij} g(\mathbf{R}_i, \mathbf{R}_j)\exp[i(\mathbf{Q}+\boldsymbol{\tau})\mathbf{R}_{ij}]. \end{aligned} \tag{10}$$

The first term in (10) is due to the long-range order and the second term is known as short-range-order (SRO) diffuse scattering expressed as the Fourier transform of the pair correlation function $g(\mathbf{R}_i, \mathbf{R}_j) = \langle S_i S_j\rangle - \langle S_i\rangle\langle S_j\rangle$.

When the system is in the disordered state, symmetry requires $g(\mathbf{R}_i, \mathbf{R}_j) = g(\mathbf{R}_i - \mathbf{R}_j)$. Then we can simplify our expression in (10) by using Cowley's SRO parameters (Warren, 1969):

$$\alpha^C(R) = 1 - p_A^\alpha(R)/c_A.$$

However, the situation is more complicated when the order parameter is not zero. Nevertheless, using symmetry arguments, we can also simplify the calculation in this case. In particular we can use $g(\mathbf{R}_{i^*}, \mathbf{R}_{j^*}) = g(\mathbf{R}_i, \mathbf{R}_j)$, if $\mathbf{R}_{i^*} = \mathbf{R}_i + \mathbf{T}$, and $\mathbf{R}_{j^*} = \mathbf{R}_j + \mathbf{T}$, where $\mathbf{T}$ is a lattice translation vector pointing from the origin of one unit cell to another. Furthermore we only need to choose an arbitrary unit cell and calculate $g(\mathbf{R}_i, \mathbf{R}_j)$ when $\mathbf{R}_i$ is within this unit cell. Each unit cell contains four atoms, which we will call A_1, A_2, A_3 and B.

We now define a new SRO parameter using the above symmetry condition

$$\begin{aligned} \alpha^s(\mathbf{R}) &= (1/4c_A c_B) g(\mathbf{R}_s, \mathbf{R}_s + \mathbf{R}) \\ &= [1/(1-m^2)] g(\mathbf{R}_s, \mathbf{R}_s + \mathbf{R}), \end{aligned} \tag{11}$$

where $k = 1, 2, 3, 4$ correspond to $\mathbf{R}_s = \mathbf{R}_{A_1}, \mathbf{R}_{A_2}, \mathbf{R}_{A_3}, \mathbf{R}_B$ in a unit cell. When the system is in the disordered state, the above parameters are equal to Cowley's SRO parameter $\alpha^C(\mathbf{R})$:

$$\alpha^s(\mathbf{R}) = \alpha^C(\mathbf{R}). \tag{12}$$

Above the phase-transition temperature T_c the diffuse scattering can be calculated using the newly defined short-range-order parameters,

$$\begin{aligned} S(\mathbf{Q})_{\mathrm{SRO}} &= \sum_{ij} (\langle f_i f_j\rangle - \langle f_i\rangle\langle f_j\rangle)\exp[i(\mathbf{Q}+\boldsymbol{\tau})\mathbf{R}_{ij}] \\ &= N c_A c_B \tilde{f}^2 \sum_i \alpha^s(\mathbf{R}_i)\exp[i(\mathbf{Q}+\boldsymbol{\tau})\mathbf{R}_i], \end{aligned} \tag{13}$$

where $\alpha^s(\mathbf{R}_i)$ take corresponding s values from 1 to 4, when $\mathbf{R}_i = \mathbf{R}_{A_1}, \mathbf{R}_{A_2}, \mathbf{R}_{A_3}, \mathbf{R}_B$ is in the unit cell.

4. *Surface X-ray intensities*

To calculate X-ray intensities under glancing-angle conditions as shown schematically in Fig. 1, we need to change the definition for the scattering vector $\mathbf{Q}$ in the equations above and to include $|T(\varphi_i)T(\varphi_f)|^2$

in A_0 (Dietrich & Wagner, 1984; Dosch, 1987; Sinha, Sirota, Garoff & Stanley, 1988). Here φ_i and φ_f are the incident and outgoing angles of the X-ray beam, respectively. $T(\varphi_i)$ and $T(\varphi_f)$ are the transmission coefficients associated with angles φ_i and φ_f. The new scattering vector is $\mathbf{Q}=(\mathbf{q}, \kappa)$, where $\mathbf{q}$ is the two-dimensional projection of $\mathbf{K}_f-\mathbf{K}_i$ onto the xy plane, and $\mathbf{K}_i$ and $\mathbf{K}_f$ are the incident and scattered wave vectors respectively. κ is the z component of the scattering vector defined by

$$\kappa=(2\pi/\lambda)[(\sin^2\varphi_f-2\delta-2i\beta)^{1/2}+(\sin^2\varphi_i-2\delta-2i\beta)^{1/2}].$$

$\delta=1-n$, where n is the refractive index for X-rays, and β is the photoelectric absorption coefficient, $\sin^2\varphi=2\delta$ defines the critical angle φ_c for total external reflection. The imaginary part of κ yields the inverse penetration depth for the X-ray beam: $\Lambda=1/|\mathrm{Im}(\kappa)|$. In the following calculation, we assume that the X-ray wavelength is $\lambda=1{\cdot}5$ Å, and that the alloy is Cu_3Au. Under these conditions $S(\mathbf{Q})$ for the long- and short-range-order parts is

$$S(\mathbf{Q})=\tfrac{1}{4}(f_{Au}-f_{Cu})^2\times\Big|\sum_f \eta(z)\exp[i(\mathbf{q}+\boldsymbol{\tau})\mathbf{r}_i]\exp[i(\kappa+\tau_z)z_i]\Big|^2+\tfrac{1}{4}(f_{Au}-f_{Cu})^2\sum_{ij} g(\mathbf{R}_i,\mathbf{R}_j)\exp[i(\mathbf{q}+\boldsymbol{\tau})\mathbf{r}_{ij}]\times\exp[i(\kappa+\tau_z)z_i]\exp[-i(\kappa^*+\tau_z)z_j], \quad (14)$$

where $\mathbf{r}=(R_x, R_y)$ is the two-dimensional projection of $\mathbf{R}$ in the xy plane.

In order to compare with the bulk case, we also define a short-range-order parameter as a function of the layer position z below the surface,

$$\alpha^s(\mathbf{R}, z)=[1-m(z)^2]^{-1}g(\mathbf{R}_s, \mathbf{R}_s+\mathbf{R}). \quad (15)$$

For the SRO diffuse scattering it follows that

$$S(\mathbf{Q})_{SRO}=c_Ac_B(f_{Au}-f_{Cu})^2\sum_{ij}\alpha^k(\mathbf{R}_i, z)\times\exp[i(\mathbf{q}+\boldsymbol{\tau})\mathbf{r}_{ij}]\exp[i(\kappa+\tau_z)z_i]\times\exp[-i(\kappa^*+\tau_z)z_j], \quad (16)$$

where $\alpha^s(\mathbf{R}_{ij}, z)$ take corresponding s values from 1 to 4, when $\mathbf{R}_i=\mathbf{R}_{A_1}, \mathbf{R}_{A_2}, \mathbf{R}_{A_3}, \mathbf{R}_B$ is in the unit cell.

In calculating the X-ray intensity, we have assumed that the sample is semi-infinite in the z direction. For the first 15 layers we used the simulation results derived from the film case and we treated the deeper layers as bulk, which is proper for the temperature range considered here which is not too close to T^*. When the temperature is very close to T^*, finite size effects have to be taken into account. In that case one has to use more layers in the z direction than we have used here.

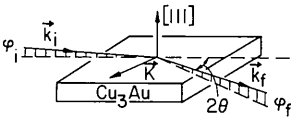

Fig. 1. Scattering geometry under grazing-incident-angle conditions.

III. Results and discussion

1. *Order parameters and concentration profiles*

In Fig. 2 the order parameter of the bulk system is shown. Our simulation reproduces a first-order-type phase transition at T^* of $1{\cdot}76(3)\ J/k_B$. This transition is in good qualitative agreement with experimental results of Keating & Warren (1951) for the bulk transition. In Table 1 we list the average short-range-order parameters, $\alpha(\mathbf{R})=[\alpha^1(\mathbf{R})+\alpha^2(\mathbf{R})+\alpha^3(\mathbf{R})+\alpha^4(\mathbf{R})]/4$, defined above [see (11)], for different temperatures. In the disordered state they are identical to Cowley's short-range-order parameters, and agree qualitatively with the measurements of Cowley (1950) and Moss (1964). In the ordered state, we also find good qualitative agreement of our calculated SRO parameters with those experimentally obtained by Chipman (1956) and Schwartz & Cohen (1965). Fig. 3 shows the calculated X-ray diffuse scattering intensity for temperatures above T^*, which also reproduces the main features of the experimental data (Cowley, 1950; Moss, 1964).

Now we discuss results which include surface effects. In Fig. 4 order-parameter profiles are shown for three different ratios of the surface-to-bulk interaction: $J_1/J=0{\cdot}5$, $1{\cdot}0$, and $2{\cdot}0$. Since our lattice contains 30 layers with two surfaces, the layer n is equivalent to layer $30-(n-1)$. For the order parameter we have taken the average of layer n and layer $30-(n-1)$. The temperature range considered here is not very close to T^*, and is about 13 K away from T^* in Cu_3Au. In this case, the 'surface region' is

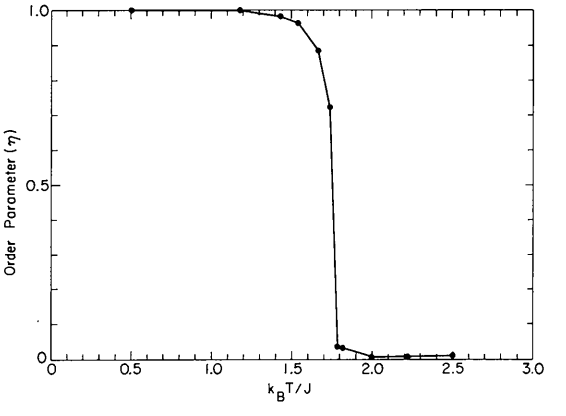

Fig. 2. Order parameter from the Monte Carlo simulation of a bulk A_3B alloy.

Table 1. *Short-range-order parameters for the simulation of the bulk phase transition*

i represents the ith neighbor atom from an atom at the origin.

i	$T=0{\cdot}812T^*$	$T=0{\cdot}874T^*$	$T=0{\cdot}947T^*$	$T=1{\cdot}033T^*$	$T=1{\cdot}136T^*$	$T=1{\cdot}263T^*$	$T=1{\cdot}420T^*$
1	−0·002	−0·005	−0·027	−0·179	−0·170	−0·157	−0·145
2	0·001	0·003	0·030	0·200	0·176	0·143	0·121
3	0·000	0·000	0·001	0·027	0·029	0·031	0·025
4	0·000	0·001	0·011	0·058	0·045	0·030	0·025
5	0·000	0·000	−0·008	−0·066	−0·057	−0·043	−0·034
6	0·000	0·000	0·002	−0·007	−0·013	−0·017	−0·012
7	0·000	0·000	−0·001	−0·006	−0·004	−0·003	−0·003
8	0·000	0·000	0·011	0·063	0·052	0·035	0·025

limited to only a few layers and finite-size effects in the z direction play no role. From this figure it appears that all layers exibit the same critical temperature independent of the interaction parameter. Clearly, $\eta(z)$ decreases at the surface and becomes rounded, *i.e.* second-order-like, with decreasing J_1/J. These order-parameter profiles also agree with the mean-field results of Lipowsky & Speth (1983) and Lipowsky & Gompper 1984) which indicate that below T^* disordered layers intervene between the vacuum and the bulk, and the number of disordered layers increases macroscopically as T approaches T^*. In our simulation the disordering of the surface layers is inferred from their reduced order parameters and is most clearly seen in Fig. 4(a) with a ratio of $J_1/J=0{\cdot}5$.

Fig. 5 shows the concentration profile for the A atom (Cu) as a function of the layer number n for three different values of J_1/J, and for two different temperatures above and below T^*. From this graph it can be seen that for $J_1/J>1$ a dramatic increase of Cu atoms in the first layer occurs. *Vice versa*,

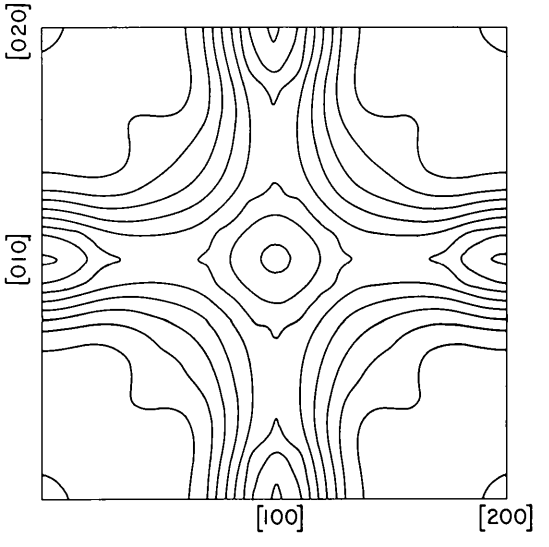

Fig. 3. $S(\mathbf{Q})_{SRO}$ contour map in a (100) plane from the bulk simulation results. It is normalized to the Laue monotonic scattering intensity $L_{Laue}=Nc_Ac_B(f_B-f_A)^2$ (Warren, 1969). The temperature corresponds to $T=1{\cdot}033T^*$.

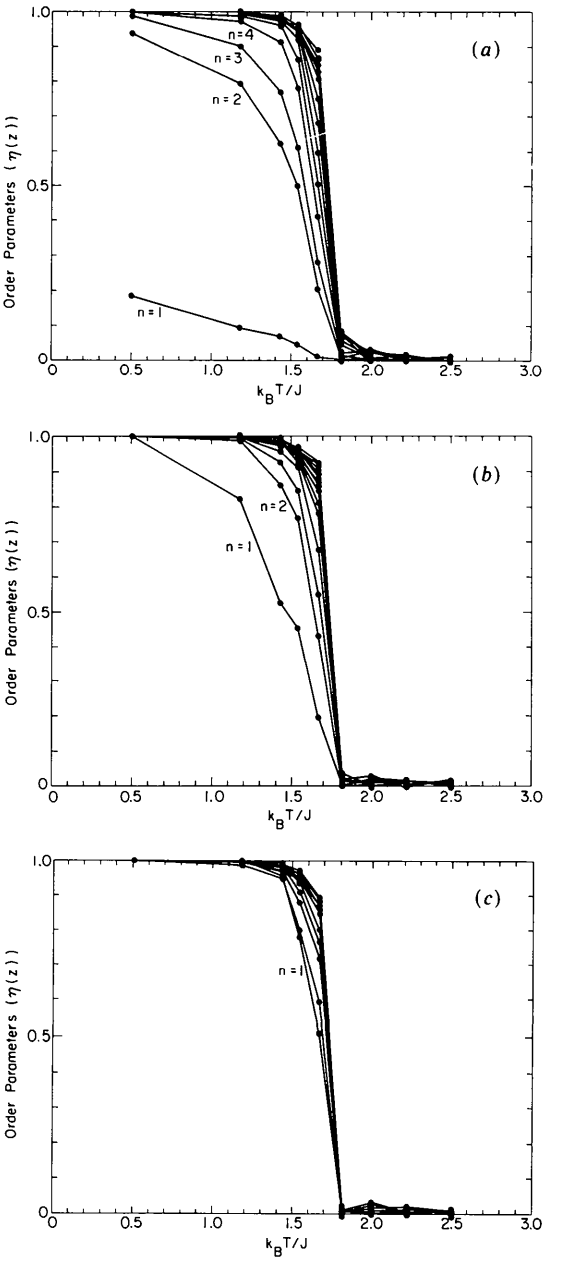

Fig. 4. Order-parameter profiles as a function of the temperature and for $J_1/J=$ (a) 0·5 (b) 1·0 (c) 2·0, and for layer $n=1$ (surface) to $n=15$.

Table 2. *Short-range-order parameter for different layers at* $T = 0{\cdot}874T^*$

i	Layer 1	Layer 2	Layer 3	Layer 4	Layer 5	Layer 6	Layer 7
1	−0·068	−0·045	−0·037	−0·023	−0·018	−0·008	−0·004
2	0·162	0·094	0·076	0·019	0·011	0·006	0·002
3	−0·004	−0·009	0·000	0·000	0·000	0·000	0·000
4	0·233	0·126	0·009	0·006	0·004	0·002	0·000
5	−0·0009	−0·115	−0·006	−0·005	−0·003	0·000	0·000
6	0·174	0·094	0·001	0·000	0·000	0·000	0·000
7	−0·022	−0·019	0·000	0·000	0·000	0·000	0·000
8	0·147	0·076	0·010	0·007	0·002	0·000	0·000
9	−0·002						
10	0·011						
11	0·002						
12	0·000						

Table 3. *Short-range-order parameters of the surface layer* ($n = 1$) *and for different temperatures and interaction parameters*

	$T = 0{\cdot}874T^*$			$T = 1{\cdot}033T^*$		
i	$J_1/J = 0{\cdot}5$	$J_1/J = 1{\cdot}0$	$J_1/J = 2{\cdot}0$	$J_1/J = 0{\cdot}5$	$J_1/J = 1{\cdot}0$	$J_1/J = 2{\cdot}0$
1	−0·142	−0·109	−0·134	−0·129	−0·168	−0·238
2	0·193	0·131	0·110	0·155	0·191	0·142
3	0·033	0·010	0·036	0·034	0·039	0·139
4	0·030	0·034	0·020	−0·024	0·031	−0·082
5	−0·055	−0·035	−0·031	−0·048	−0·066	−0·055
6	−0·020	−0·007	0·019	−0·006	−0·041	−0·054
7	0·001	−0·002	−0·022	0·031	0·001	−0·035
8	0·053	0·042	0·032	0·015	−0·007	0·043
9	0·004	−0·003	0·009	−0·001	0·010	0·056
10	0·018	0·018	0·021	−0·009	0·019	0·016
11	0·001	0·000	−0·005	0·001	0·004	0·012
12	0·004	0·000	0·033	−0·007	−0·003	0·066

$J_1/J < 1$ results in a depletion of Cu atoms in the surface layer.

In Table 2 we reproduce the average short-range-order parameter $\alpha = [\alpha^1(\mathbf{R}, z) + \alpha^2(\mathbf{R}, z) + \alpha^3(\mathbf{R}, z) + \alpha^4(\mathbf{R}, z)]/4$ for each layer from $n-1$ to 7 at $T = 0{\cdot}874T^*$ and for the interaction parameter ratio $J_1/J = 1{\cdot}0$. Note that only the first few layers exhibit SRO parameters which are significantly different from the bulk values.

Table 3 lists the average SRO parameters (as defined in Table 2) of the surface layer ($n = 1$) and for different temperatures and interaction parameters. Here it becomes obvious that while the SRO parameters are roughly the same at the surface and in the bulk for $T > T^*$, for $T < T^*$ they are considerably larger at the surface than in the bulk.

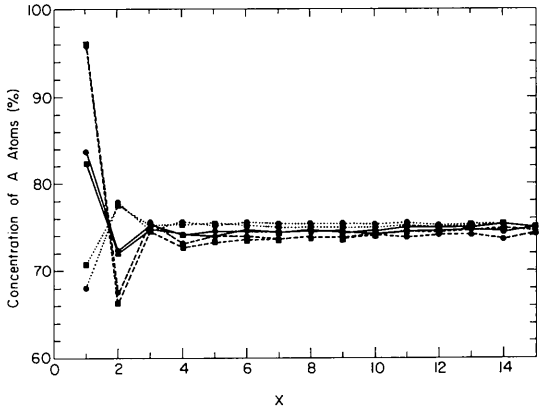

Fig. 5. Concentration profiles for Cu atoms as a function of layer index n. Squares represent $T = 1{\cdot}033T^*$, circles $T = 0{\cdot}947T^*$. The dashed lines are for $J_1/J = 0{\cdot}5$, solid lines for $J_1/J = 1{\cdot}0$, and dotted lines for $J_1/J = 2{\cdot}0$.

2. *Surface X-ray scattering for* Cu_3Au (111) *ordered alloys*

(*a*) *Long-range order.* Fig. 6 shows the calculated $S(\mathbf{Q})$ due to the long-range order assuming a

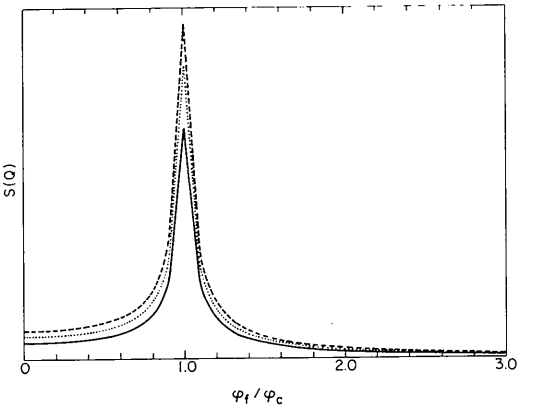

Fig. 6. $S(\mathbf{Q})_{\mathrm{LRO}}$ under grazing-incident scattering conditions. The incident angle φ_i is fixed at the critical angle φ_c. The x axis represents the exit angle φ_f in terms of φ_c. The dashed line is for $T = 0{\cdot}661T^*$; dotted line $T = 0{\cdot}874T^*$; solid line $T = 0{\cdot}947T^*$.

grazing-incidence scattering geometry as shown in Fig. 1. In this plot, the incident angle φ_i is constant and chosen to be identical to the critical angle φ_c for the total external reflection, while the exit angle φ_f is scanned. For this calculation it is also assumed that $J_1/J=1$. For $\varphi_f<\varphi_c$ a smooth intensity drop is observed with increasing temperature towards T^*, while for $\varphi_f>\varphi_c$ the intensity change is much smaller over the same temperature range. This difference just reflects the fact that, closer to the surface, the order parameter decreases more smoothly than deeper in the bulk, which is in good qualitative agreement with the X-ray work of Dosch *et al.* (1988). A direct comparison is however not possible since their measurements were taken on a (100) surface of Cu_3Au.

We have also calculated the LRO X-ray intensity along the (100) truncation rod for a (111) surface. As we described before,

$$S(\mathbf{Q})_{\mathrm{LRO}}=\tfrac{1}{4}(f_A-f_B)^2\left|\sum_i \eta(z)\exp\left[i(\mathbf{q}+\boldsymbol{\tau})\mathbf{r}_i\right]\right.$$
$$\left.\times\exp\left[i(\kappa+\tau_z)z_i\right]\right|^2. \qquad (17)$$

For our case $\tau=(100)$ and $\exp(i\tau_z z_i)=(-1)^{n_3}$. After summing over all positions in the xy plane we obtain

$$S(\mathbf{Q})=\tfrac{1}{4}(f_A-f_B)^2N_1^2N_2^2$$
$$\times\left|\sum_{n_3}\eta(n_3)(-1)^{n_3}\exp(i\kappa n_3 a_3)\right|^2, \qquad (18)$$

where a_3 is the distance between (111) planes, and $z=a_3n_3$. For the LRO parameters $\eta(n_3)$ we used the results of the MC simulation shown in Fig. 4.

The results are shown in Fig. 7. For an ideal infinite lattice, the X-ray intensity would appear as Bragg spots. But because of the surface and finite penetration depth in the z direction, the Bragg peak actually extends in the κ_z direction and forms a so-called truncation rod (Robinson, 1986). This type of diffuse rod exists for both fundamental and superlattice reflections. If the order parameter of successive layers is not uniform, the shape of the superlattice truncation rod will change accordingly. This presents an alternative way to study order-parameter profiles. As can be seen from a comparison of the truncation rods in Fig. 7 plotted for different temperatures, the intensity along κ is very sensitive to the details of the phase transition and the LRO both at the surface and in the bulk.

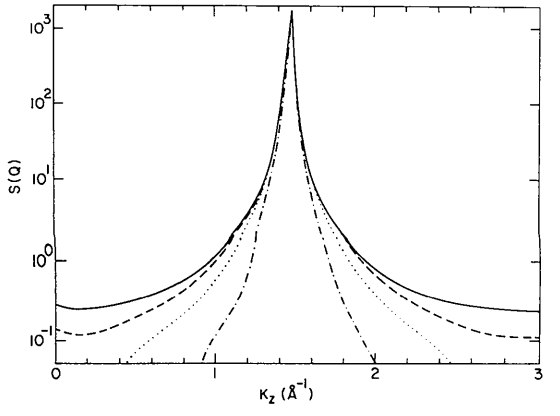

Fig. 7. $S(\mathbf{Q})$ for the truncation rod of the 100 peak for different temperatures, assuming $\varphi_i=\varphi_f=\varphi$ and $J_1/J=1$. The intensity is normalized to $\frac{1}{4}(f_A-f_B)^2N_1^2N_2^2$ and is plotted as a function of $\kappa_z=(4\pi/\lambda)\sin\varphi$. The solid line is for $T=0{\cdot}284T^*$, dashed line for $T=0{\cdot}668T^*$, dotted line for $T=0{\cdot}812T^*$ and chain-dotted line for $T=0{\cdot}947T^*$.

(*b*) *Short-range-order diffuse scattering.* Figs. 8(*a*) and (*b*) show a contour map of the SRO diffuse scattering expected for grazing-incidence scattering conditions and for glancing angles $\varphi_i=\varphi_f=0{\cdot}75\varphi_c$. For these angles the X-ray penetration depth is about

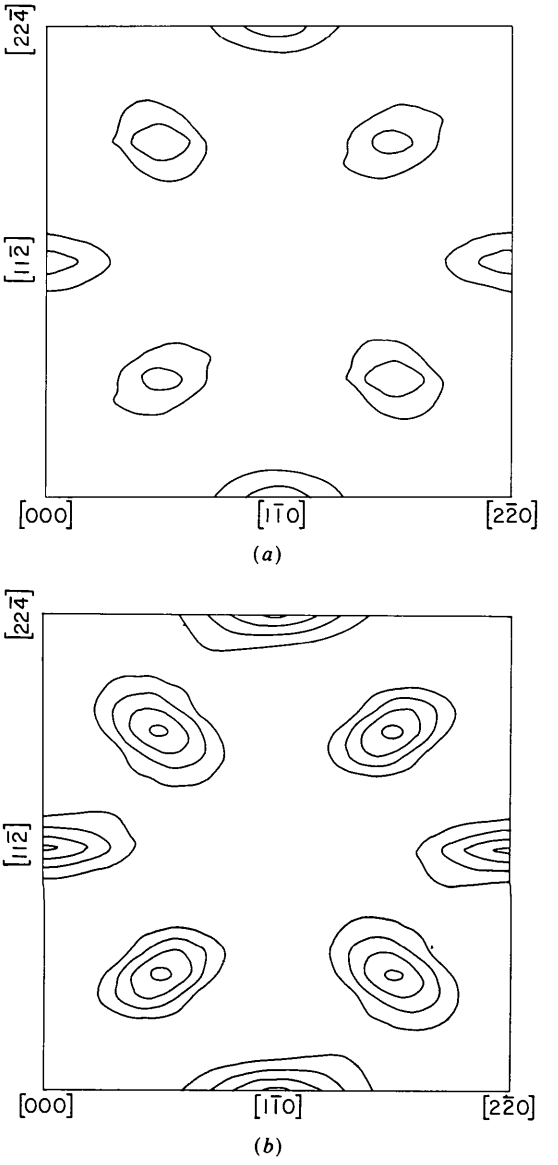

Fig. 8. $S(\mathbf{Q})_{\mathrm{SRO}}$ contour map under glancing-angle conditions with $\varphi_i=\varphi_f=0{\cdot}75\varphi_c$, for (*a*) $T=0{\cdot}874T^*$ and (*b*) $T=1{\cdot}033T^*$.

10 layers deep. The temperatures are $T = 0{\cdot}874T^*$ and $1{\cdot}033T^*$ in Figs. 8(a) and (b), respectively. For $T > T^*$, there is no significant difference between surface and bulk layers and the SRO diffuse scattering is mainly from bulk-like layers. However, at $T = 0{\cdot}874T^*$, the main contribution to the SRO diffuse scattering originates in the surface region which extends now over approximately four layers, while the SRO parameters of the bulk-like layers are essentially equal to zero (see Table 1). Therefore, only for $T < T^*$ can valuable information on the surface SRO be gained in a glancing-angle X-ray experiment.

In Fig. 9 the calculated $S(\mathbf{Q})$ SRO diffuse due to scattering is shown for a scan along the exit angle φ_f while keeping the incident angle fixed at $\varphi_i = \varphi_c$. Below T^* (dashed line) the intensity is weak for $\varphi_f < \varphi_c$, increases at $\varphi_f = \varphi_c$ and decreases slowly with increasing φ_f. This is because, for $T < T^*$, the SRO diffuse intensity originates mainly in a limited number of surface layers, and increasing the exit scattering angle does not enhance the scattering intensity much. On the other hand, above T^* the diffuse intensity is higher for all exit angles, because above T^* the SRO of the bulk makes an important contribution to the total diffuse intensity.For large φ_f the SRO diffuse scattering intensity, corresponding to the Fourier transform of the pair correlation in the z direction, decreases slowly with increasing φ_f due to a loss of pair correlation in the z direction.

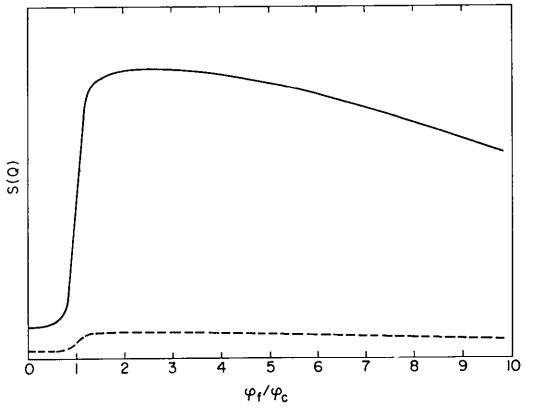

Fig. 9. $S(\mathbf{Q})_{\mathrm{SRO}}$ as a function of the exit angle φ_f for fixed incident angle $\varphi_i = \varphi_c$ and $\mathbf{q}$ at the reciprocal point $[1, \bar{1}, 0]$. Solid line is for $T = 0{\cdot}874T^*$, and dotted line for $T = 1{\cdot}136T^*$.

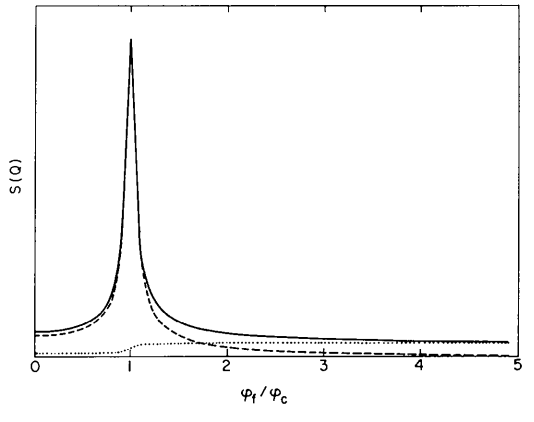

Fig. 10. $S(\mathbf{Q})_{\mathrm{LRO}}$ (dashed line), SRO intensity (dotted line), and $S(\mathbf{Q}) = S(\mathbf{Q})_{\mathrm{LRO}} + S(\mathbf{Q})_{\mathrm{SRO}}$ (solid line) is plotted as a function of the exit angle φ_f for fixed incident angle $\varphi_i = \varphi_c$ and for $\mathbf{q}$ at the reciprocal point $[1, \bar{1}, 0]$. The temperature is $T = 0{\cdot}947T^*$.

Another result from the present MC simulation worth mentioning here is that the SRO diffuse scattering of Cu_3Au in a bulk measurement below T^* is insignificant compared with the intensity due to the long-range-order parameters. Therefore, in bulk scattering experiments the SRO diffuse scattering does not need to be considered when measuring LRO parameters. However, the situation is different for surface scattering experiments. Here the total scattering intensity, as shown in Fig. 10, has to be corrected for the SRO diffuse intensity in order to obtain proper LRO parameter profiles for the surface layers.

IV. Summary

We have presented the results of a Monte Carlo simulation of an A_3B ordering alloy, specifically including surface effects. From the simulation short-range and long-range-order parameters were extracted as a function of the layer beneath the surface and for various ratios J_1/J of the surface and bulk interaction parameters.

Glancing-angle surface X-ray scattering is a sensitive probe for surface phase transitions and order-parameter profiles. The present simulation has been used to calculate the short-range- and long-range-order scattering intensities. Below the critical temperature the diffuse intensity is mainly due to surface effects, while above T^* the SRO diffuse scattering from the bulk dominates the diffraction signal. In addition, scans of the long-range-order part along surface truncation rods are shown to be highly sensitive to the long-range-order parameter profiles, which depend crucially on the interaction ratio J_1/J.

X-ray experiments for determining order-parameter profiles are currently in progress and will be reported shortly.

We have benefited from valuable discussion with D. S. Lewart concerning the computer programming. The computer simulation was carried out in the Materials Research Center for Computation within the Materials Research Laboratory. We gratefully acknowledge support from the Department of Energy, Division of Material Science, under grant DOE-AC02-76-ER01198.

References

ALS-NIELSEN, J. (1986). *Structure and Dynamics of Surfaces*, 2, edited by W. SCHOMMERS & P. VAN BLANCKENHAGEN. *Topics in Current Physics*. Berlin: Springer-Verlag.

ALVARADO, S. F., CAMPAGNA, M., FATTAH, A. & UELHOFF, W. (1987). *Z. Phys. Teil B*, **66**, 103-106.

BINDER, K. (1986). *Monte Carlo Methods in Statistical Physics*, 2nd ed., edited by K. BINDER. Berlin: Springer-Verlag.

CHEN, H., COMSTOCK, R. J. & COHEN, J. B. (1979). *Annu. Rev. Mater. Sci.* **9**, 51-86.

CHIPMAN, D. R. (1956). *J. Appl. Phys.* **27**, 739-746.

COWLEY, J. M. (1950). *J. Appl. Phys.* **21**, 24-30.

DIETRICH, S. & WAGNER, H. (1984). *Z. Phys. Teil B*, **56**, 207-215.

DOSCH, H. (1987). *Phys. Rev. B*, **35**, 2137-2143.

DOSCH, H., MAILANDER, L., LIED, A., PEISL, J., GREY, F., JOHNSON, R. L. & KRUMMACHER, S. (1988). *Phys. Rev. Lett.* **60**, 2382-2385.

EISENBERG, P. & MARRA, W. C. (1981). *Phys. Rev. Lett.* **46**, 1081-1084.

FONTAINE, D. DE (1979). *Solid State Physics*, Vol. 34, edited by H. EHRENREICH, F. SEITZ & D. TURNBULL. New York: Academic Press.

GOLOSOV, N. S. & DUDKA, B. V. (1973). *Phys. Status Solidi B*, **59**, 361-366.

GOMPPER, G. & KROLL, D. M. (1988). *Phys. Rev. B*, **38**, 459-473.

JAMISON, K. D., LIND, D. M., DUNNING, F. B. & WATTERS, G. K. (1985). *Surf. Sci.* **159**, L451-L459.

KEATING, D. T. & WARREN, B. E. (1951). *J. Appl. Phys.* **22**, 286-290.

LIPOWSKY, R. (1984). *J. Appl. Phys.* **55**, 2485-2490.

LIPOWSKY, R. & GOMPPER, G. (1984). *Phys. Rev. B*, **29**, 5213-5215.

LIPOWSKY, R. & SPETH, W. (1983). *Phys. Rev. B*, **28**, 3983-3993.

MCRAE, E. G. & MALIC, R. A. (1984). *Surf. Sci.* **148**, 551-580.

MEJIA-LIRA, F., BENNEMAN, K. H. & MORAN-LOPEZ, J. L. (1985). *Phys. Rev. B*, **32**, 5925-5931.

MOSS, S. C. (1964). *J. Appl. Phys.* **35**, 3547-3553.

POLGREEN, T. L. (1985). *Acta Metall.* **33**, 185-189.

ROBINSON, I. K. (1986). *Phys. Rev. B*, **33**, 3830-3836.

SANCHEZ, J. M., MEJIA-LIRA, F. & MORAN-LOPEZ, J. L. (1986). *Phys. Rev. Lett.* **57**, 360-363.

SANCHEZ, J. M. & MORAN-LOPEZ, J. M. (1985). *Phys. Rev. B*, **32**, 3534-3540.

SCHWARTZ, L. H. & COHEN, J. B. (1965). *J. Appl. Phys.* **36**, 598-616.

SINHA, S. K., SIROTA, E. B., GAROFF, S. & STANLEY, H. B. (1988). *Phys. Rev. B*, **38**, 2297-2311.

SORNETTE, D. (1985). *Phys. Rev. B*, **31**, 4672-4675.

WARREN, B. E. (1969). *X-ray Diffraction*. Reading, MA: Addison-Wesley.

ZHU, X.-H., FEIDENHANS'L, R., ZABEL, H., ALS-NIELSEN, J., DU, R., FLYNN, C. P. & GREY, F. (1988). *Phys. Rev. Rapid Commun. B*, **37**, 7157-7160.

Acta Cryst. (1990). A**46**, 94-98

A New Approach for *n*-Beam Dynamical Calculations

BY K. WATANABE

Tokyo Metropolitan Technical College, 1-10-40 *Higashiohi, Shinagawa-ku, Tokyo* 140, *Japan*

Y. KIKUCHI

Advanced Technology Division, Fujitsu Ltd, 1015 *Kamikodanaka, Nakahara-ku, Kawasaki-shi* 122, *Japan*

AND K. HIRATSUKA AND H. YAMAGUCHI

Department of Physics, Faculty of Science, Science University of Tokyo, 1-3 *Kagurazaka, Shinjuku-ku, Tokyo* 162, *Japan*

(*Received* 8 *March* 1989; *accepted* 1 *September* 1989)

Abstract

With the use of modulated plane waves, a new method for *n*-beam dynamical calculations has been established on the basis of a paper by Watanabe, Kikuchi, Hiratsuka & Yamaguchi [*Phys. Status Solidi A* (1988), **109**, 119-126]. The computing time is reduced to about one-sixth of what it originally was and a large reduction of memory is achieved. *n*-beam dynamical calculations of aluminium, copper and gold at several accelerating voltages and orientations were carried out in a completely parallel manner by the present method, the multi-slice method and Bethe's eigenvalue method [Fujiwara (1959). *J. Phys. Soc. Jpn* **14**, 1513-1524]. The present method turned out to be competitive with respect to accuracy and speed in comparison with the latter two methods. The new method makes *n*-beam dynamical calculations of complex systems and defects possible.

1. Introduction

After direct-lattice images from a large unit cell (Allpress, Sanders & Wadsley, 1969; Uyeda, Kobayashi, Suito, Harada & Watanabe, 1972; Hashimoto, Endo, Tanji, Ono & Watanabe, 1977) were observed by high-resolution electron microscopy, the development of electron microscopy made

0108-7673/90/020094-05$03.00